Modelling of the BS-4 Atlanta Field to Assess Fault Reactivation and the In-Situ Stresses during Production

Dr. William Ferguson[1*]
Dr. Adam Bere[1]
Dr. Carlos Suarez[2]

1. Rockfield Software Limited, Ethos Building, Kings Road, Prince of Wales Dock, Swansea, SA1 8AS, United Kingdom

2. QGEP, Av. Alimirante Barroso, 11o Andar, Centro, RJ-CEP 220031-918, Rio de Janeiro, Brazil.

*. Corresponding author. Email: w.ferguson@rockfield.co.uk

Abstract

QGEP are the operators of the BS-4 Atlanta Field and are principally concerned with the potential of faults reactivating and propagating through to the seabed during production. This paper presents a three-dimensional finite element geomechanical numerical simulation to assess the fault reactivation and the general field stress distribution during a 30 year period of production. The BS-4 Atlanta field geometry was constructed as a geomechanical model with the simulation carried out in terms of total stress. The presented simulation was undertaken by Rockfield used their own in-house *Elfen Coupled Reservoir Geomechanics* software suite. A network of 54 pre-existing faults was incorporated into the model and was represented using double-sided surfaces and discrete element contact which permits actual slip to occur. A two-stage modelling strategy was applied; pre-production and production. The pre-production stage aims to capture the current-day material and stress states of the BS-4 field accounting for geometric variability, material characteristics, salt creep and stress realignment due to the presence of the pre-defined faults. Current-day stress results are presented which show a good agreement with minifrac experimental results. The production stage captures the geomechanical response of the field arising from depletion; the stress distribution, sea floor deformation and fault slip are presented. Additionally, a dynamic assessment of sand production is presented along proposed well trajectories throughout the full duration of the 30 year production period.

Introduction

The Atlanta field lies within the BS-4 block of the Santos Basin and is located approximately 185 km offshore from the Rio de Janeiro Province in Brazil, Figure 1. QGEP is the operator of the BS-4 block and expect to start production in late 2014/early 2015. Prospect NE lies in the north central section of the BS-4 block and consists of a 4 way dipping structure associated with geological salt deformation in the basin. The prospective sequence consists of Eocene to Albian deepwater turbidite sandstones, Figure 2; the primary objectives are the Eocene and Upper Albian turbidite deposits. A robust flat spot in the Eocene corresponds to a readily identified structural trap with the high probability of encountering hydrocarbons at that depth.

Figure 1

Figure 2

QGEP are principally concerned with potential seafloor deformation that will affect the operation of subsea equipment and that faults may be reactivated and propagate through to the seafloor during production. Therefore, the principal objective of this study is to assess the geomechanical response of the BS-4 field during production and the assessment of fault reactivation, fault propagation and seafloor deformation.

This paper presents a three-dimensional simulation of the BS-4 Atlanta field to assess the potential fault movement that will be encountered during production. The fault network within the field is represented within the model with double-sided surfaces and discrete contact which permits sliding of the faults to occur; fault movement is assessed by the relative movement of the adjacent fault sides.

A two-stage modelling strategy is used to determine the in-situ stress evolution during depletion; pre-production stress and production. The pre-production stage aims to capture the material and stress state of the BS-4 field prior to production accounting for equilibrium of horizontal stresses due to variations in lateral stresses, salt creep and the reorientation of stresses around faults. The effect of reservoir depletion on the in-situ stresses and its impact upon faults slip is predicted in the production stage. The presented methodology for the geomechanical modelling of reservoirs enables the effect of different depletion scenarios on fault reactivation and stress distribution to be rapidly assessed.

A depletion scenario is simulated for the BS-4 Atlanta field which assumes no aquifer underlying the reservoir. The initial and production pore pressure distributions were supplied by QGEP from a reservoir simulation and imposed directly upon the geomechanical models. The BS-4 Atlanta field geometry was constructed as a geomechanical model with the simulation carried out in terms of total stress. The presented simulation was undertaken by Rockfield using their own in-house *Elfen Coupled Reservoir Geomechanics* software suite.

Material Characterisation

The supplied horizons provide the upper and lower limits of the field stratigraphy; however, the stratigraphy represented in the geomechanical model was refined based upon well log data. The following regions were retained as distinct strata:

- **Unconsolidated Mud:** The top 50m is comprised of weak unconsolidated mud.
- **Overburden:** The overburden is comprised of fairly monotonous claystones (Griffiths, 2001)
- **Reservoir:** The reservoir is the region of predominant interest. This section consists of a sequence of highly porous, but also unconsolidated sands.
- **Underburden:** This stratum is generally a sand, silt, claystone and limestone interbedded sequence; the sands and claystones dominate in the upper and lower sections respectively (Griffiths, 2001). This section was further divided into two strata as defined below.
- **Albian:** Albian is a sand dominated formation with silty claystones as interbeds (Griffiths, 2001); no well log data exists at these depths consequently, material properties were assumed based on Rockfield's experience.
- **Salt:** The underlying salt is a viscoelastic material which will creep due to imposed deviatoric stresses.

Figure 3 shows the bulk density and the compression wave travel times from Figure 3well 1-SHEL-4-RJS at depths in the range 2000 – 4000m TVDMSL; there is a marked change in the well log data at approximately the Disc IV horizon indicating a change in the response of the material. Two materials were defined in the region between Albian and the reservoir; these are termed underburden (upper) and underburden (lower) with the boundary at the Disc IV horizon.

Figure 3

The stratigraphy of the geomechanical model is comprised of seven materials listed with increasing depth as; unconsolidated mud, overburden, reservoir, underburden (upper), underburden (lower),

Albian and salt. Table 1 shows the relationship between the model stratigraphy and the supplied horizons.

Table 1

The objective of the material characterisation is to determine the mechanical properties of the strata used for the geomechanical modelling of the BS-4 Atlanta field. The determination of the material properties is principally based upon the supplied experimental and log data; however, where no experimental or well log data was available, values were based upon Rockfield experience. Data exists for the uppermost 50m of the field *Unconsolidated Mud* (Fugro-McClelland Marine Geosciences Inc, 2006) with well log data available from *1-SHEL-4* (Griffiths, 2001). The strata are represented within the numerical model by pressure- or porosity-dependent elastic material model; the characterisation provides upper and lower bound properties for each material; upper and lower-bound properties refer to the material strength. A summary of the characterised formation properties is shown in Table 2.

Table 2

A salt body underlies the BS-4 Atlanta field at depths of approximately 3320 – 6780m TVDMSL. The salt is modelled using a steady state Munson-Dawson material model (Munson, 1997); this material model includes steady state creep terms and temperature dependent visco-plasticity. Avery Island material parameters for the salt were assumed (Fossum and Fredrich, 2001); Avery Island properties represent *average* salt behaviour and are typically used world-wide in the absence of field specific data. The steady state strain rate of Avery Island (located in the Gulf of Mexico) is of the same order of magnitude as creep tests conducted on salt from Brazil (Costa *et al*), consequently, in the absence of supplied data for the salt, it was considered by Rockfield that Avery Island salt is a suitable representation of the salt underlying the Atlanta field.

The temperature varies linearly with depth from 4°C at the seabed and increasing by 3.61°C per 100m (Fugro-McClelland Marine Geosciences Inc, 2006). The bulk density of the salt body is assumed to be 2100 kg/m^3; the bulk density is assumed to be similar to that in the Franco and Libra fields which are approximately 65 km away.

Three-Dimensional Model

The modelled domain is approximately 25 km × 25 km × 5 km with the reservoir at a depth of approximately 2400m TVDMSL and the seabed located at 1500m TVDMSL. The three-dimensional model of the BS-4 field is shown in Figure 4. The depletion region is approximately central to the modelled domain and is bounded to the West by fault principal.

Figure 4

The fault network was supplied by QGEP as a series of 54 point clouds from which the fault planes were generated. The modelled fault network, Figure 5, is dominated by a graben which has formed above a ridge of the underlying salt body, Figure 6; the graben is bounded by fault principal and fault anti-C1W which are aligned NE-SW

Figure 5

Figure 6

The pre-defined faults within the BS-4 domain are modelled with double-sided discrete contact which permits sliding of the faults to occur. A Coulomb friction law is assumed for the faults; the Coulomb friction law within Rockfield's in-house software *Elfen* is written in terms of the normal and tangential effective stresses on the faults. A cohesion and coefficient of friction of 0 MPa and 0.2 respectively were used for the Coulomb friction law applied to the faults; fault properties were selected at the lower end of a realistic range.

Modelling Methodology

The modelling methodology for evaluating the stress evolution and fault movement during production is completed in two phases:

- Pre-production.
- Production.

Both phases consider total stress assumptions.

Pre-Production

The pre-production phase aims to capture the material and the stress state of the BS-4 field immediately prior to production. This will ensure that during production, the modification of stresses is accurately represented such that the elastic response and any potential yielding are captured. Two modelling stages are required to generate the current-day pre-production stress:

- Initialisation.
- Equilibrium.

Initialisation is based upon the application of stress and material states from known data:

- Assignment of the porosity variation with depth. The initial porosity for the reservoir varied both across the domain and with depth and was extracted directly from the supplied data and imposed upon the reservoir stratum within the model. The porosity for the underburden (upper) varied with depth whereas for all other strata the initial porosity was constant as defined in Table 2.
- Assignment of pore pressures; the pore pressure is modelled as hydrostatic from mean sea level with a constant fluid density of 1025 kg/m^3..
- Automatic application of vertical effective stress. The vertical effective stress is determined automatically and based upon the total weight of the overlying material considering both the porosity and the grain density.
- Assignment of the horizontal effective stress based on the calculated effective vertical stress and the coefficient of lateral earth pressure assigned to each layer within the model. The assigned

coefficients of lateral earth pressure are given in Table 3 and were based upon the anticipated three-dimensional effects of the field geometry.

Table 3

The objective of the *equilibrium* phase is to predict the current day pre-production stress and material state throughout the BS-4 Atlanta field by accounting for the following:

- Geometric variability.
- Material characteristics.
- Equilibrium of horizontal stresses due to variations in assigned coefficients of lateral earth pressures.
- Stress realignment due to the presence of predefined faults.
- Salt creep.

The models were permitted to reach quasi-static equilibrium, following initialisation; this evolves the stress and material state from the initialised condition to the pre-production condition. At the end of the equilibrium stage, the model is considered to be representative of pre-production conditions within the Sandia field and suitable for reservoir depletion simulations.

Production

The aim of the production stage is to predict the deformation, stress distribution and fault slip that will occur within the BS-4 field during the depletion of the reservoir. The variation in pore pressure due to depletion is imposed upon the model and its impact is assessed. Therefore, due to consideration of total stress assumptions, modification of the pore pressure results in modification of the effective stress.

Results and Discussion

The following section presents the pre-production stress distribution and also the evolution of the stress and the fault movement arising from production. Additionally, the reservoir depletion simulation enables an assessment of sand production along proposed well trajectories to be carried out; a sanding assessment for the BS-4 field is presented.

Current Day

Figure 7 and Figure 8 present the current-day maximum compressive total stress and the ratio between the vertical total and maximum compressive principal stress respectively. The ratio of the stresses is approximately 0.97 above the reservoir implying that the that the maximum compressive total principal stress is aligned within 15° of the vertical in this region of the field; beneath the reservoir the stress ratio is unity giving the direction of the maximum compressive total principal stress as vertical.

Figure 7

Figure 8

The orientation of the minimum compressive horizontal stress is shown in Figure 9 within the overburden and at the top of the Albian. The orientations of the minimum horizontal stress are SE(-30º) and NNE(60º) within the overburden and Albian respectively; these values have not changed significantly during the equilibrium stage indicating a good equilibrium of the in-situ stresses. Local reorientation of the stresses occurs directly adjacent to the fault network; in this region the horizontal stresses are approximately isotropic and hence no preferential direction for the minimum horizontal stress.

Figure 9

Two salt ridges are evident within the BS-4 field, Figure 6, and their evolution results in the following:

- The generation of the *graben* bounded by fault principal and fault anti C1W.
- Flexure of the overburden.

Flexure of the overburden, resulting from the evolution of the salt ridge, causes the rotation of the minimum horizontal stress with depth. This process is analogous to the bending of a beam with a stress reversal occurring about the neutral axis of the beam. A schematic diagram of this process and its relation to BS-4 is given in Figure 10. In summary, the orientation of the minimum horizontal stress varies with depth due to bending of the overburden:

- The *maximum* horizontal stress is aligned normal to the salt ridge immediately above the salt body.
- The *minimum* horizontal stress is aligned normal to the salt ridge and fault principal in the layers above the reservoir; the *maximum* horizontal stress is parallel to fault principal.

Three minifrac experimental tests (Pedrosa, 2013) were performed on the pilot well 9-RJS-ATL-1D to determine the minimum horizontal stress within the reservoir of the BS-4 field. The tests were carried out within the reservoir sandstone formation at a depth of 7635ft (2327m) TVD. Analysis of the pressure variation with time yields fracture gradients of 0.5097 psi/ft, 0.5090 psi/ft and 0.5088 psi/ft at the instantaneous shut-in pressure. The report (Pedrosa, 2013) concluded that the average closing pressure or minimum horizontal stress was 3885 psi (26.786 MPa).

The minifrac test results were used to validate the stress distribution determined by the numerical simulation; Table 4 presents a comparison of the numerical and experimental minimum horizontal stress at the minifrac test location. The minimum horizontal total stress determined by the 3D model was in the range 3949 psi (27.23 MPa) – 4028 psi (27.77 MPa) at depths of 7601 – 7651ft (2317 – 2332m) TVD. There is a good agreement between the experimental and simulation current-day stress results; the 3D simulation results overestimate the minimum horizontal total stress by only 1.7 – 3.7%.

Table 4

Production

The following section presents the seafloor deformation and fault slip following 30 years of production; these are the areas of principal concern to QGEP. Additionally, the potential for sand production along proposed well trajectories is presented.

The depletion pressures were determined by QGEP from a reservoir simulation; Figure 11 shows the depletion region and the depletion with time at selected points on section AA.

Figure 11

Figure 12 depicts the variation in the vertical deformation after 30 years of production; the vertical deformation at the sea floor, within the overburden and at the top of the reservoir is shown in Figure 13. There is negligible deformation beneath the reservoir, however, significant vertical deformation is evident between the sea floor and the base of the reservoir and is confined to the region immediately above the depletion zone. The maximum vertical deformation is approximately 1.9m and occurs directly above the reservoir depletion zone; the maximum deformation of the sea floor is approximately 1.4m. The reservoir of the BS-4 Atlanta field is relatively shallow at a depth of approximately 800 – 900 m beneath the sea floor; consequently little stress arching occurs within the overburden resulting in the magnitude and lateral extent of the vertical deformation of the sea floor being similar to that at the reservoir. The effective vertical stress within the reservoir becomes more compressive during depletion and results in the vertical compaction of the reservoir; lateral compaction also occurs.

Figure 12

Figure 13

Figure 14 presents various views of the fault network with the fault slip that occurs after 30 years of production plotted. Fault slip takes place within and directly adjacent to the depletion zone; fault slip is not significant at a distance from this region. The maximum fault slip is 0.82m and occurs on fault dip25; which lies on the eastern boundary of the depletion region. In general, fault slip:

- Tends to be greatest within the vertical bounds of the reservoir.
- Occurs within and above the reservoir.
- Below the reservoir, fault slip is not significant.

Figure 14

The evolution of fault slip is shown in Figure 15; the locations are selected to highlight the greatest fault slip. The most active faults are fault principal and fault dip25 which bound the depletion region on the western and eastern sides respectively. Fault slip is related directly to the rate of production within the reservoir:

- Gradual fault slip occurs during the first 5 years of production.
- A significant increase in the rate of fault slip occurs after approximately 5 years and is attributed to a significant increase in the rate of production (additional production wells to be brought online).

- The rate of fault slip gradually decreases between 5 and 30 years as the rate of production decreases, Figure 11.

Figure 15

The distinction of fault slip after 30 years of production is shown in Figure 16. In general, normal faulting is evident within the BS-4 field assuming non-aquifer depletion. However, thrust faulting occurs on fault principal, fault C2E2 and fault E2E1 extended on the western boundary of the depletion zone. This reversal of faulting type is characterised by:

- Normal faulting below the reservoir.
- Thrust faulting in the region between the sea floor and the reservoir.
- A *neutral axis* located along the upper surface of the reservoir; fault slip is negligible along the *neutral axis*.

The variation of faulting type is shown in Figure 17 for selected East-West sections.

Figure 16

Figure 17

Sanding Assessment

An assessment of sand production was carried out on a series of proposed well trajectories, Figure 18, over the full duration of the 30 year production period. The principal stresses and the pore pressures were extracted from the three-dimensional model along the length of the supplied well trajectories.

Figure 18

The location of the highest deviatoric stress on each of the wellbore trajectories was selected for sanding assessment. The circumferential stress around the proposed wellbore was determined using the Kirsch equation (Weijermars, 2011) with the extracted model stresses. The maximum permissible drawdown was evaluated as:

$$dd_{max} = \sigma_{\theta\, yield} - \sigma_{\theta} \tag{1}$$

where dd_{max}, σ_{θ} and $\sigma_{\theta\, yield}$ are the maximum permissible drawdown, circumferential stress on the well (evaluated from the model and varying with depletion) and the yield stress of the formation respectively.

Results for sanding assessment are presented as the bottomhole flowing pressure variation with the reservoir pressure. Typical results are presented in Figure 19 which is comprised of two curves:

1. Reservoir pressure. The reservoir pressure is a straight line where the bottomhole flowing pressure is equal to the reservoir pressure – this indicates zero drawdown conditions.

2. Critical bottomhole flowing pressure (CBHFP). The CBHFP is the minimum bottomhole flowing pressure that can be achieved without sand production for a given reservoir pressure. The CBHFP is defined as:

$$CBHFP = P_{reservoir} - dd_{max} \tag{2}$$

where $P_{reservoir}$ is the reservoir pressure. Sand-free oil production can be achieved if the bottomhole flowing pressure exceeds the CBHFP; the range of permissible bottomhole flowing pressures for a given reservoir pressure for sand-free production is termed the *operating envelope*. Sand production will occur if the bottom hole flowing pressure falls below the CBHFP.

The CBHFP is non-linear because the evolution of the stress state during depletion is considered during its' evaluation.

Figure 19

The sanding assessment for the proposed well trajectories considering both the best and worst case wellbore orientations are presented in Figure 20 and Figure 21. The assessment assumes all wells to be horizontal, cased and perforated and that the reservoir has a thick-walled cylinder strength of 5.5 MPa. All wells will be sand-free during production if the well is aligned parallel to the minimum horizontal stress (best-case well orientation). Conversely, if the wells are aligned parallel to the maximum horizontal stress (worst-case well orientation), sand will potentially be produced in all wells; Wells P08 and P04 exhibit the greatest and least potential for sand production at a reservoir pressure of approximately 19 MPa and 13 MPa respectively.

Figure 20

Figure 21

A qualitative sanding assessment has been presented which highlights a benefit of numerical simulation of reservoir depletion. In order, to assess quantitatively the likelihood of sand production in the proposed wells, thick-walled cylinder tests (or potentially UCS data) are required to determine accurately the formation strength.

Conclusions

This paper has presented a three-dimensional numerical simulation of the geomechanical response of the BS-4 Atlanta field for a 30 year period of production; also presented was the pre-production stress distribution and a comparison against minifrac experimental test data. The principal findings of this study are:

- The evolution of the salt ridge underlying the BS-4 field has formed the *graben* bounded by fault principal and fault anti- C1W. Additionally, the salt ridge has resulted in the bending of the overburden and a change in the orientation of the pre-production minimum horizontal stress with depth:
- Vertical compaction of the reservoir occurs due to depletion; compressibility of the reservoir is the major influence on fault slip.
    - The rate and magnitude of fault slip is directly related to the rate and magnitude of the reservoir depletion.
    - In general, normal faulting occurs within the BS-4 field. However, thrust faulting occurs for the non-aquifer case on fault principal, fault C2E2 and fault E2E1 Extended on the western boundary of the depletion zone; normal faulting occurs below the reservoir with thrust faulting above.
    - The maximum fault slip is 0.82m and occurs on fault dip25 after 30 years of production.
- The maximum vertical deformation on the reservoir and the sea floor is 1.9 m and 1.4 m respectively. The reservoir within the BS-4 field is relatively shallow at a depth of approximately 800 – 900 m below the mudline; consequently, stress arching is not significant and the magnitude of the displacements at the seafloor are a similar magnitude to the displacements at the reservoir.
- A qualitative assessment of sand production was undertaken on proposed well trajectories which highlight the impact of well orientation; experimental TWC data is required to carry out a quantitative sanding assessment.

References

Costa, A.M., Poiate, E., Amaral, C.S., Goncalves, C.J.C., Falcao, J.L. and Pereira, A., [2010], Geomechanics applied to the well design through salt layers in Brazil: A history of success*, presented at the 44th US Rock Mechanics Symposium and the 5th US-Canada Rock Mechanics Symposium,* Salt Lake City, June 27-30.

Fossum, A.F. and Fredrich, J.T. [2001], Salt mechanics primer for near salt and sub-salt deepwater Gulf of Mexico field developments, Sandia Report, SAND2001-xxxx.

Fugro-McClelland Marine Geosciences Inc [2006], Geotechnical Investigation BS-4 Field Santos Basin, Offshore Brazil, Report 0201-5672-2.

Griffiths, H. [2001],Wellsite Geology and Wireline Data End of Well Report Exploration Well 1-SHEL-4/4A-RJS, Shell Deepwater Services, Report EP2001-4059.

Munson, D.E. [1997], Constitutive model of creep in rock salt applied to underground room closure, *International Journal for Rock Mechanics and Mining Science*, **34(2)**, 233 – 247.

Pedroso, C.A., [2013] *Relatório de Microfraturamento do Poço 9-ATL-1D-RJS*.

Weijermars, R. [2011], Analytical stress functions applied to hydraulic fracturing: Scaling the interaction of tectonic stress and unbalanced borehole pressures, *45th US Rock Mechanics and Geotechnics Symposium*, San Francisco.

List of Figure Captions

Figures

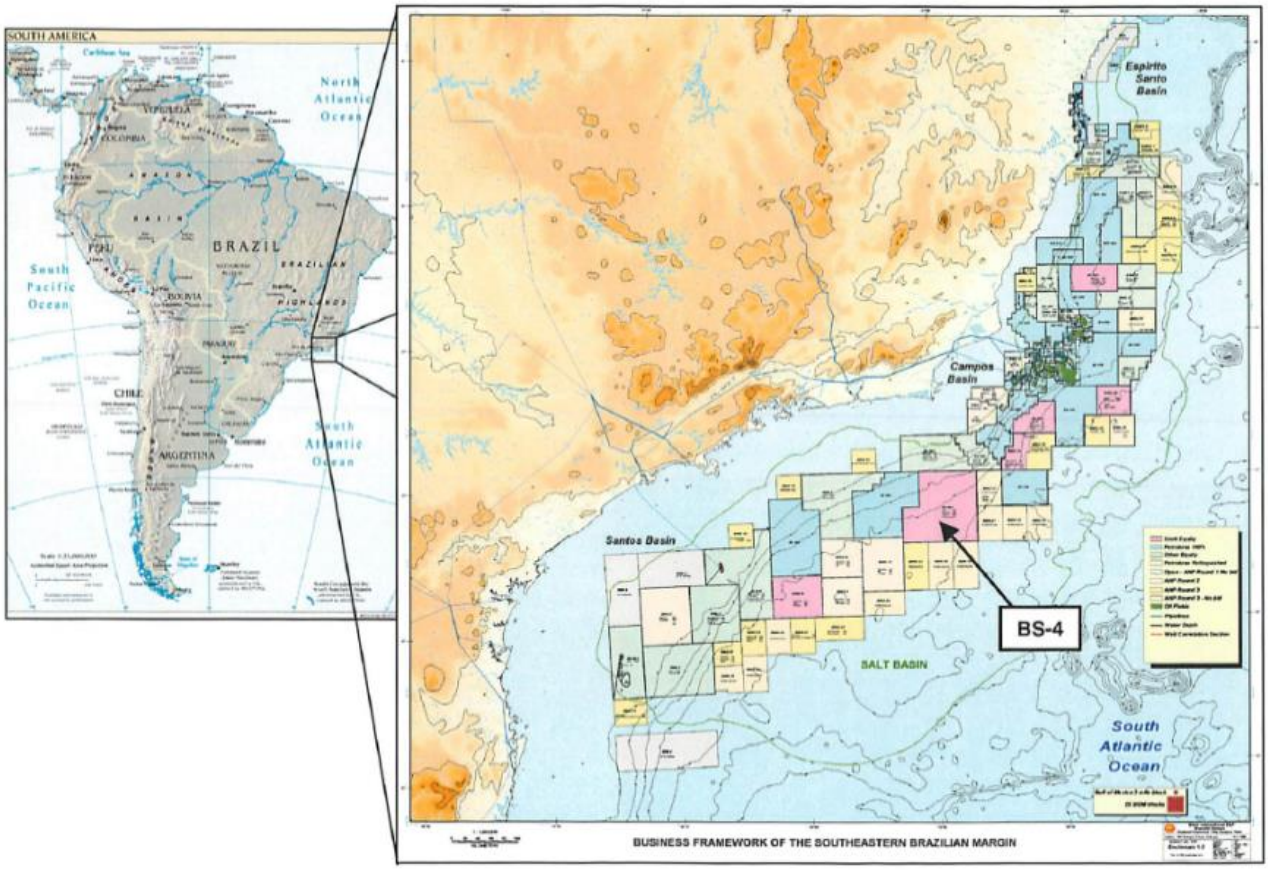

Figure 1

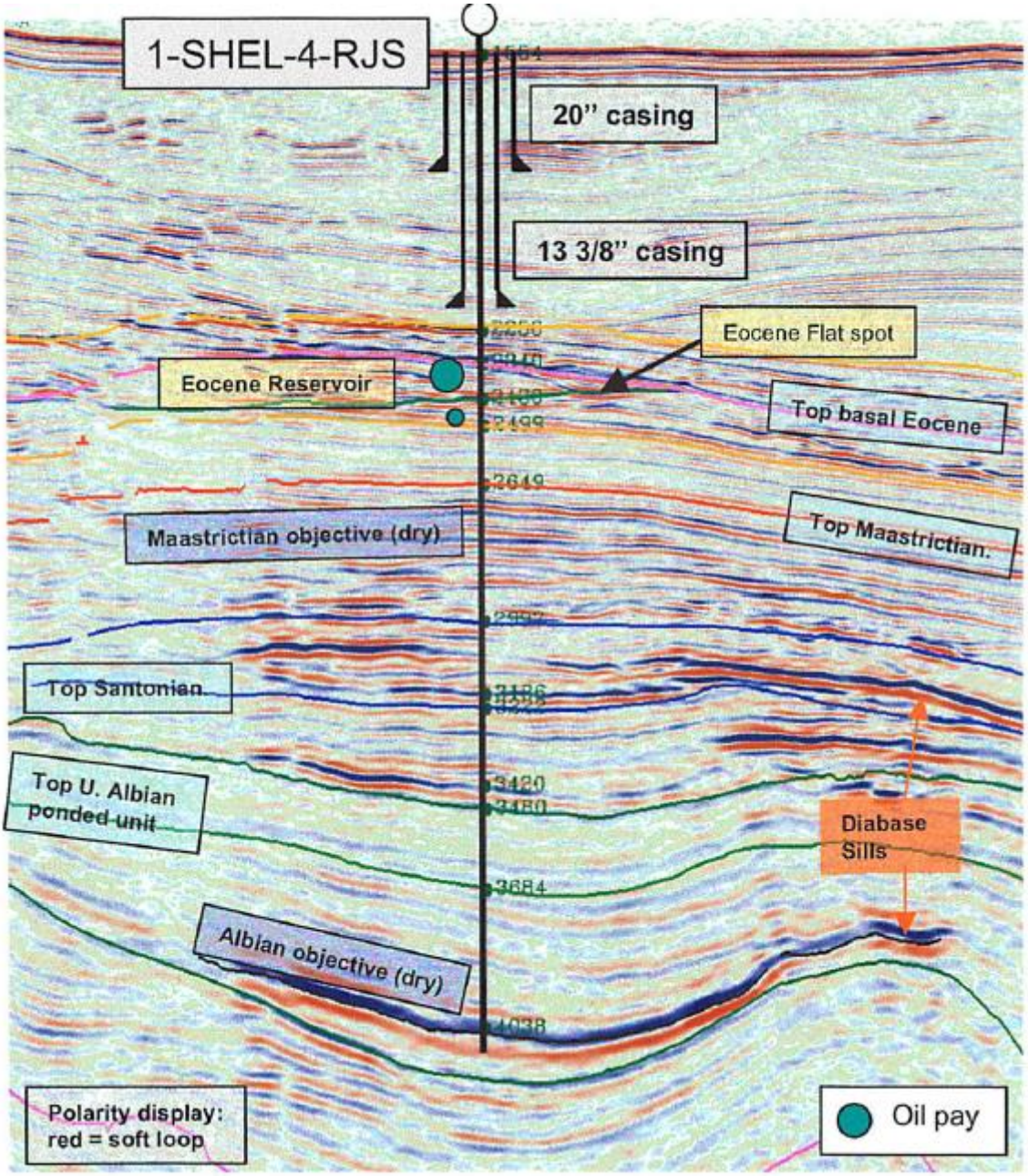
1-SHEL-4-RJS
20" casing
13 3/8" casing
Eocene Flat spot
Eocene Reservoir
Top basal Eocene
2649
Maastrictian objective (dry)
Top Maastrictian.
Top Santonian
3420
Top U. Albian ponded unit
Diabase Sills
3684
Albian objective (dry)
4038
Polarity display: red = soft loop
Oil pay

Figure 2

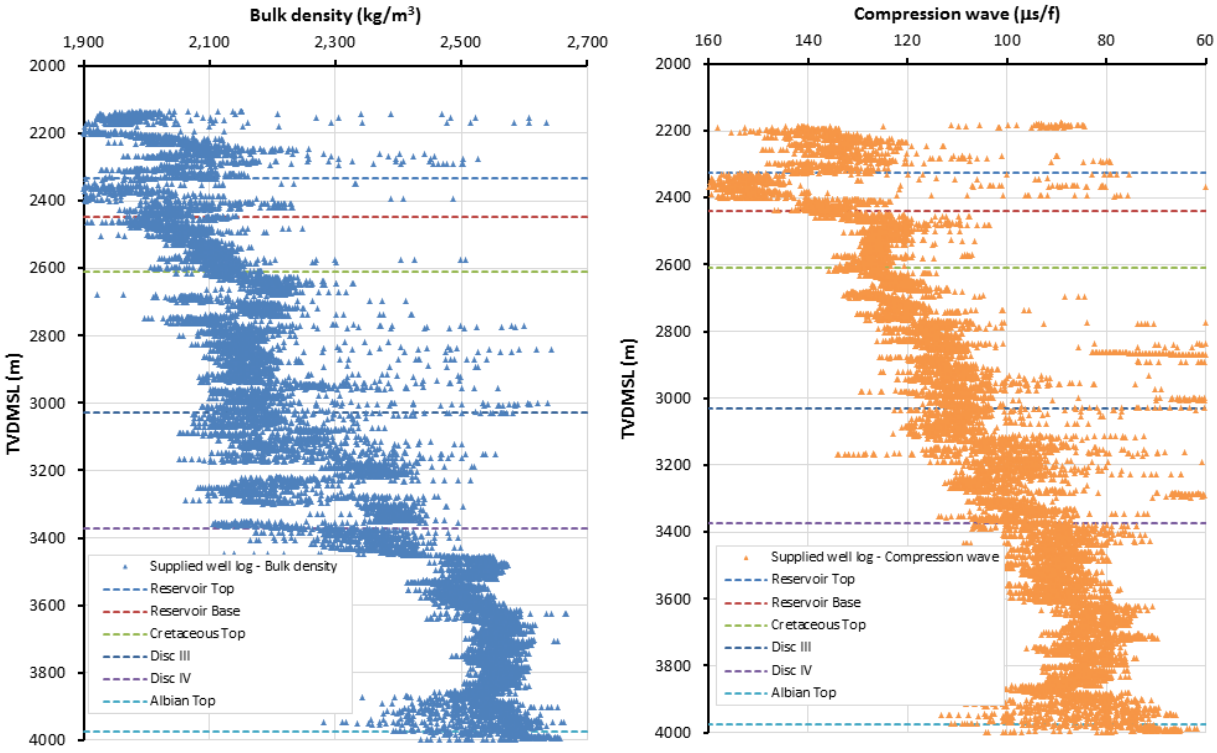
Bulk density (kg/m³)
1,900
2,100
2,300
2,500
2,700
TVDMSL (m)
2000
2200
2400
2600
2800
3000
3200
3400
3600
3800
4000
Supplied well log - Bulk density
Reservoir Top
Reservoir Base
Cretaceous Top
Disc III
Disc IV
Albian Top
Compression wave (µs/f)
160
140
120
100
80
60
TVDMSL (m)
Supplied well log - Compression wave
Reservoir Top
Reservoir Base
Cretaceous Top
Disc III
Disc IV
Albian Top

Figure 3

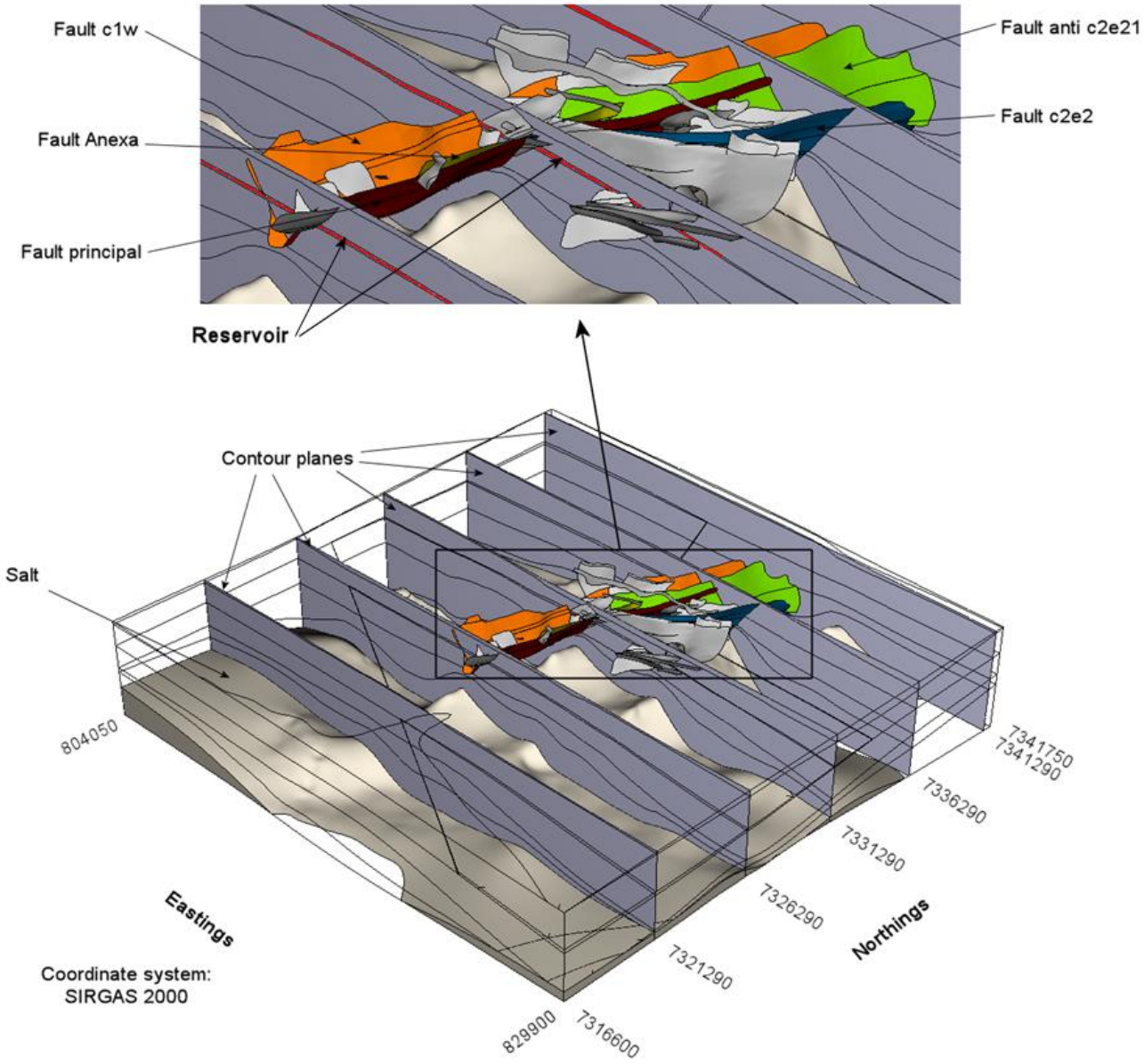
Fault c1w
Fault anti c2e21
Fault c2e2
Fault Anexa
Fault principal
Reservoir
Contour planes
Salt
804050
7341750
7341290
7336290
7331290
7326290
7321290
7316600
829900
Eastings
Northings
Coordinate system:
SIRGAS 2000

Figure 4

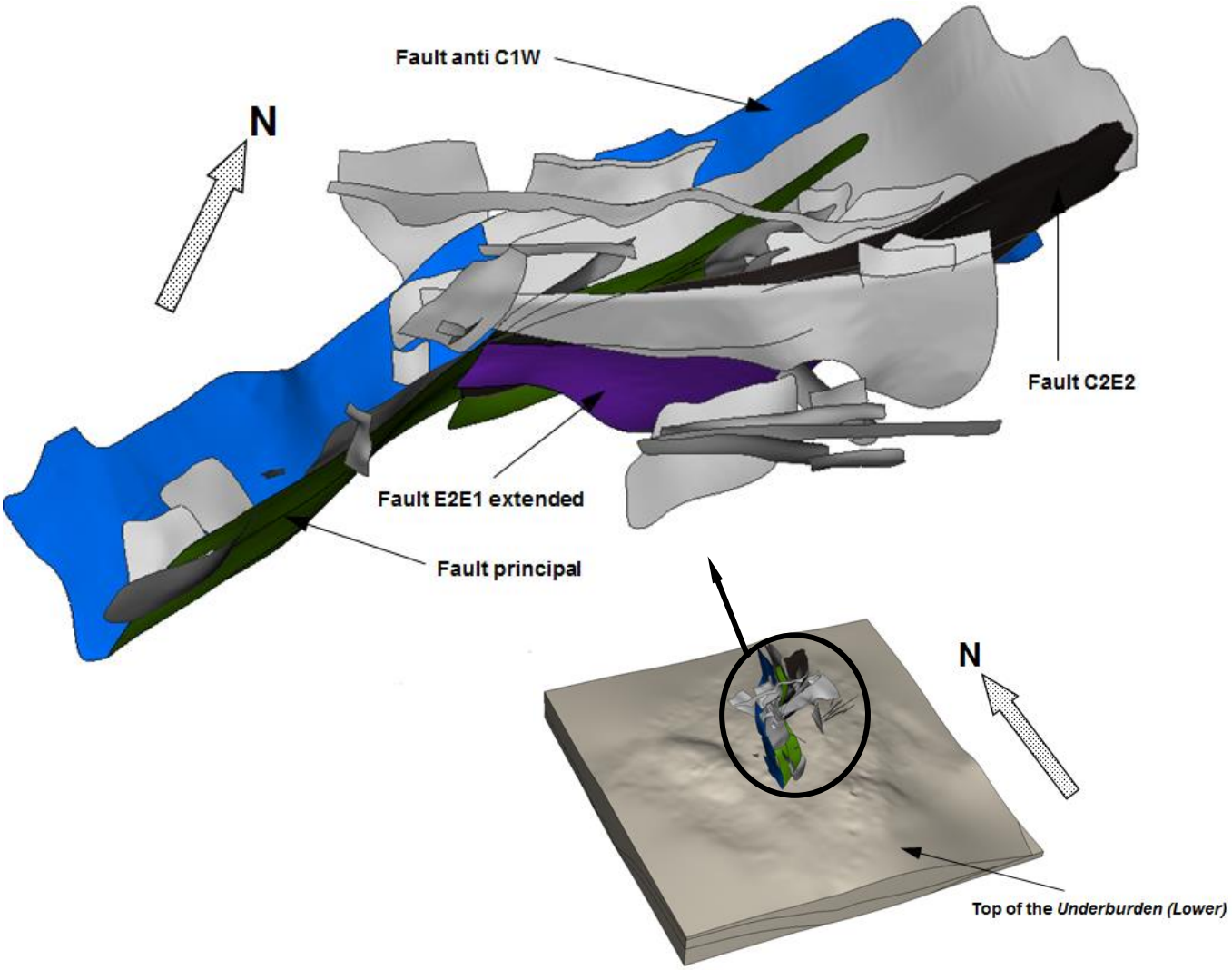
Fault anti C1W
N
Fault C2E2
Fault E2E1 extended
Fault principal
N
Top of the *Underburden (Lower)*

Figure 5

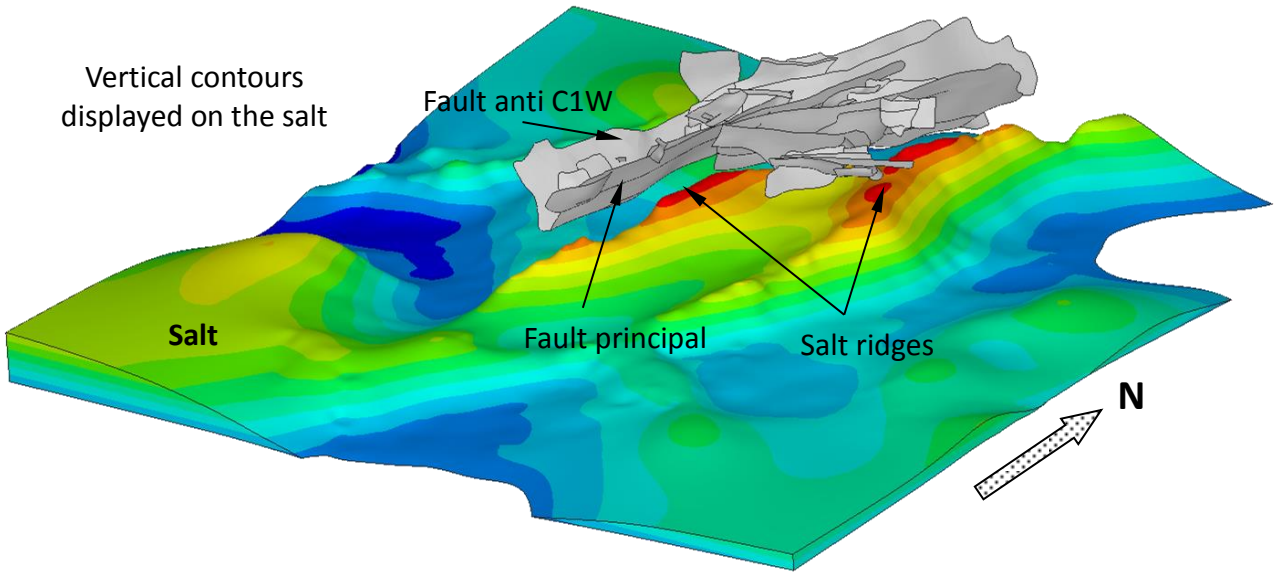
Vertical contours
displayed on the salt
Fault anti C1W
Salt
Fault principal
Salt ridges
N

Figure 6

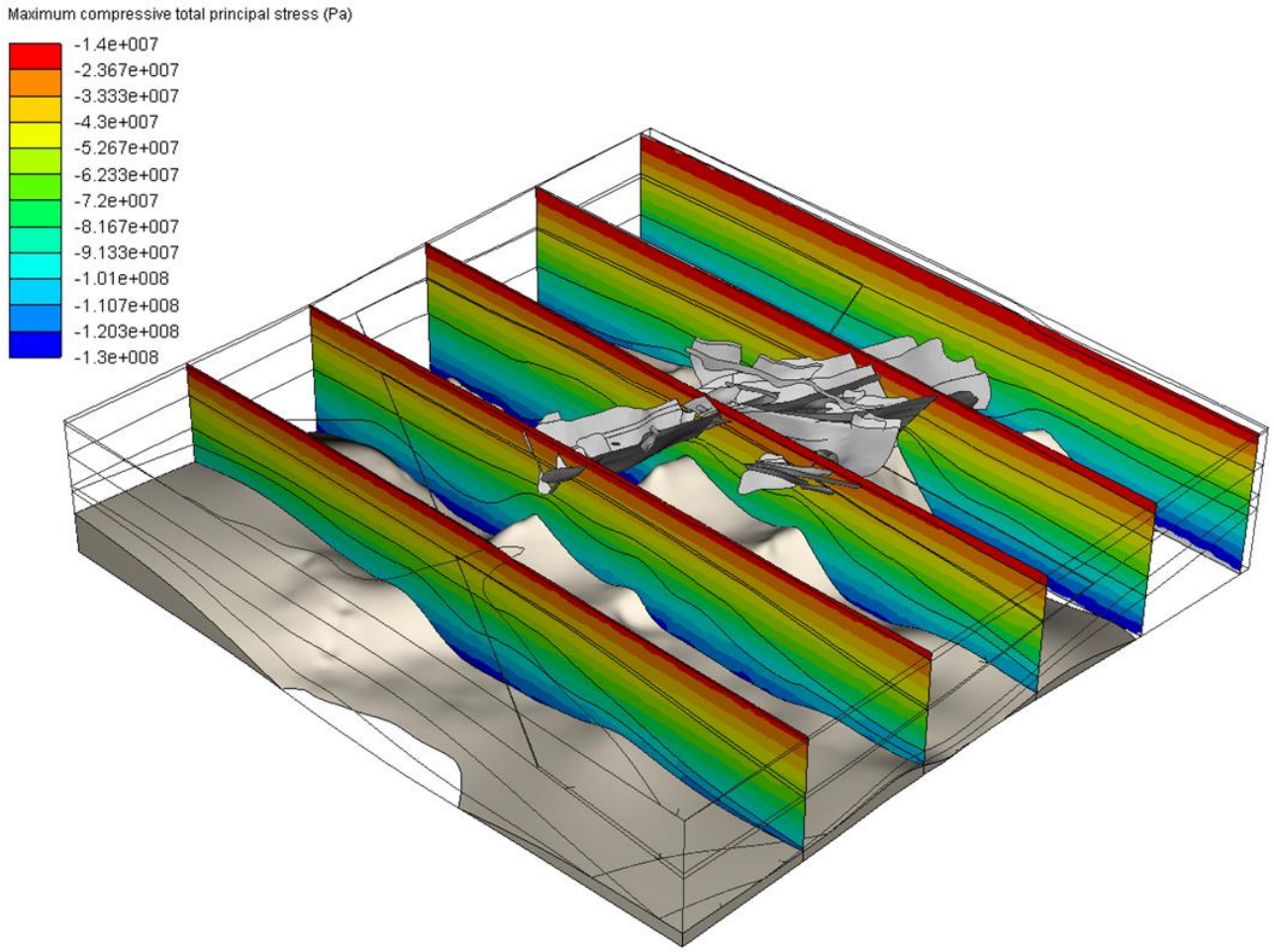
Maximum compressive total principal stress (Pa)
-1.4e+007
-2.367e+007
-3.333e+007
-4.3e+007
-5.267e+007
-6.233e+007
-7.2e+007
-8.167e+007
-9.133e+007
-1.01e+008
-1.107e+008
-1.203e+008
-1.3e+008

Figure 7

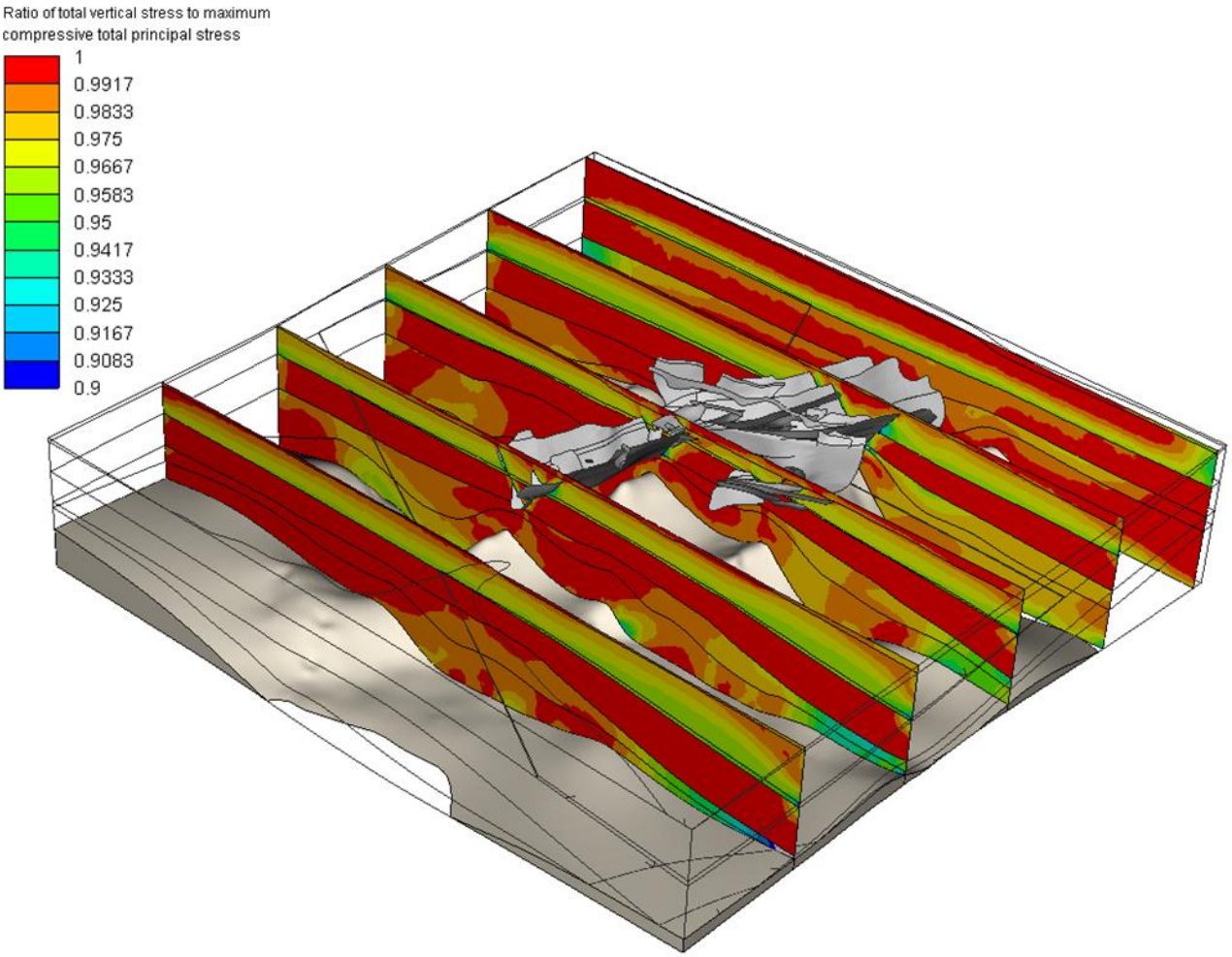
Ratio of total vertical stress to maximum compressive total principal stress
1
0.9917
0.9833
0.975
0.9667
0.9583
0.95
0.9417
0.9333
0.925
0.9167
0.9083
0.9

Figure 8

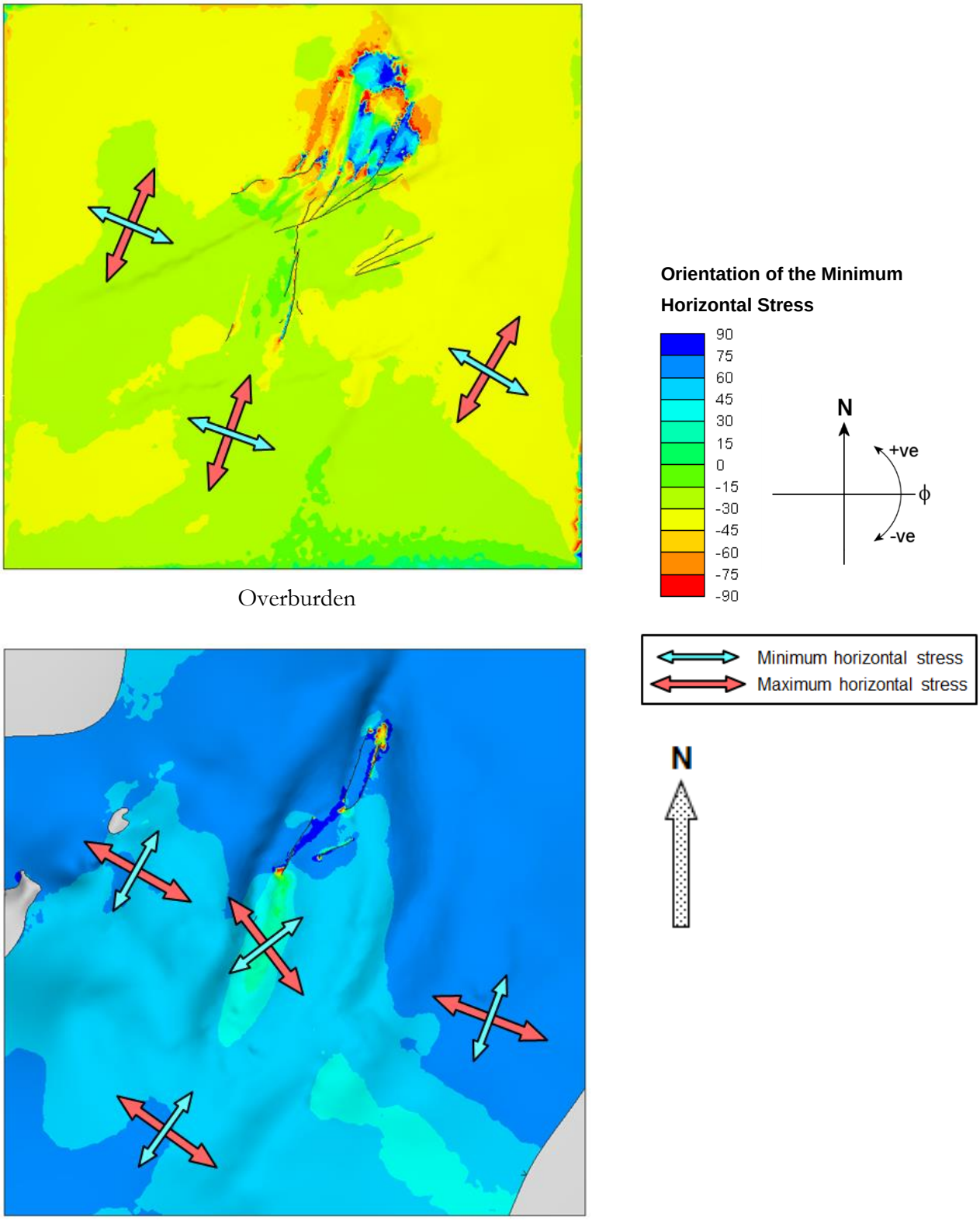

Overburden

Albian

Figure 9

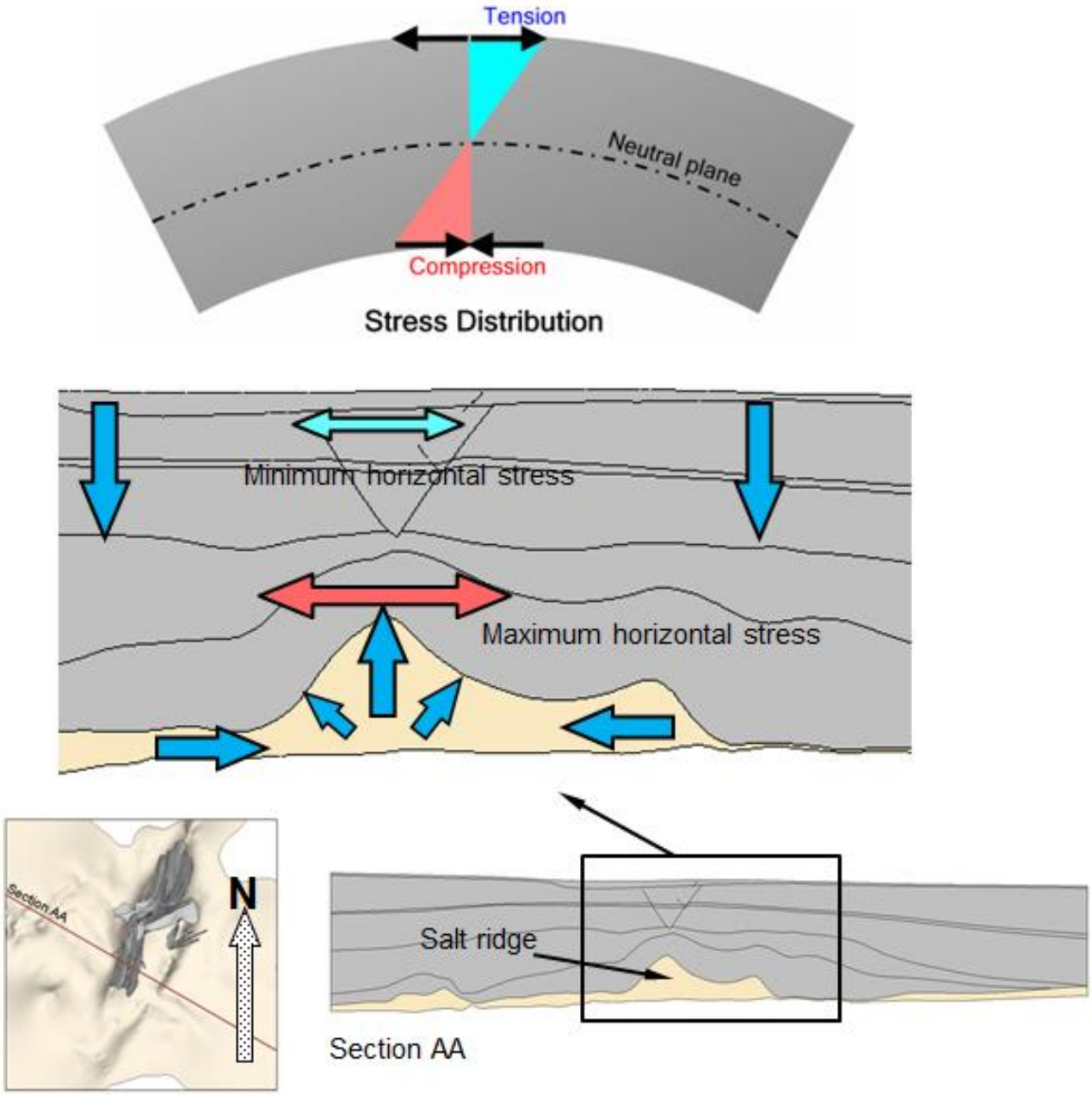
Tension
Neutral plane
Compression
Stress Distribution
Minimum horizontal stress
Maximum horizontal stress
Section AA
N
Salt ridge
Section AA

Figure 10

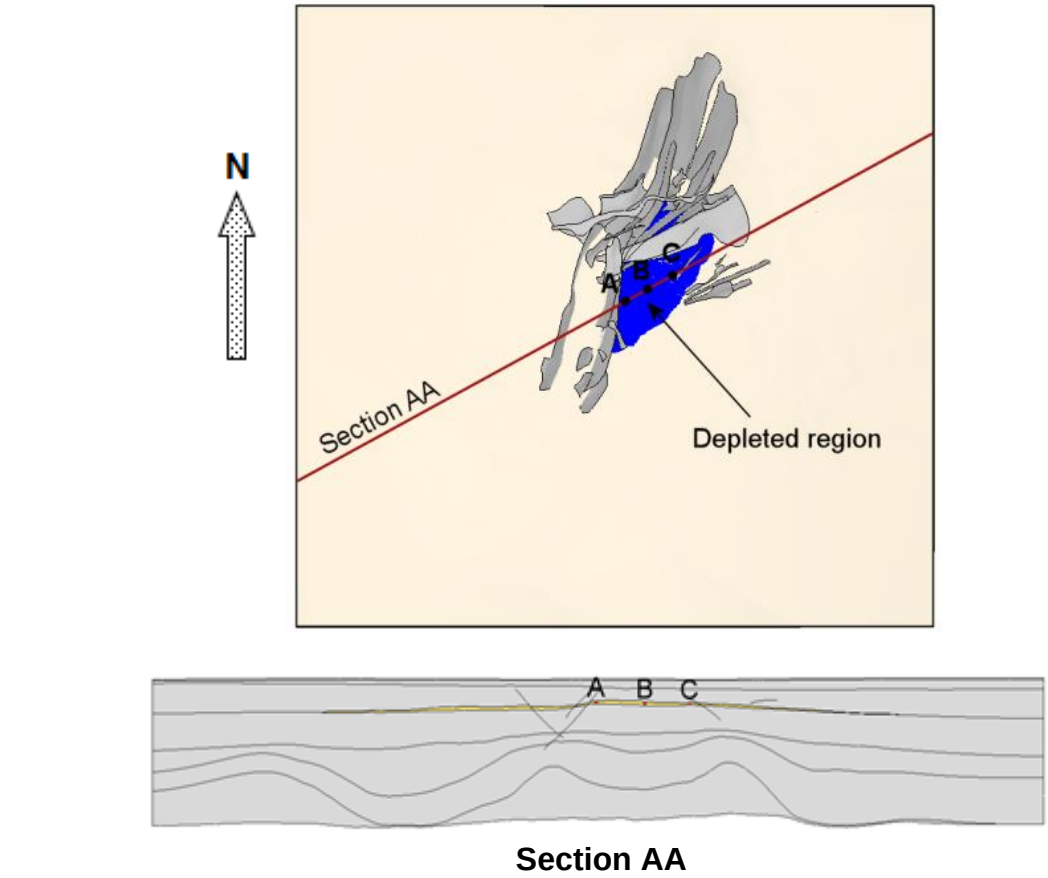
N
A
B
C
Section AA
Depleted region
A B C
Section AA

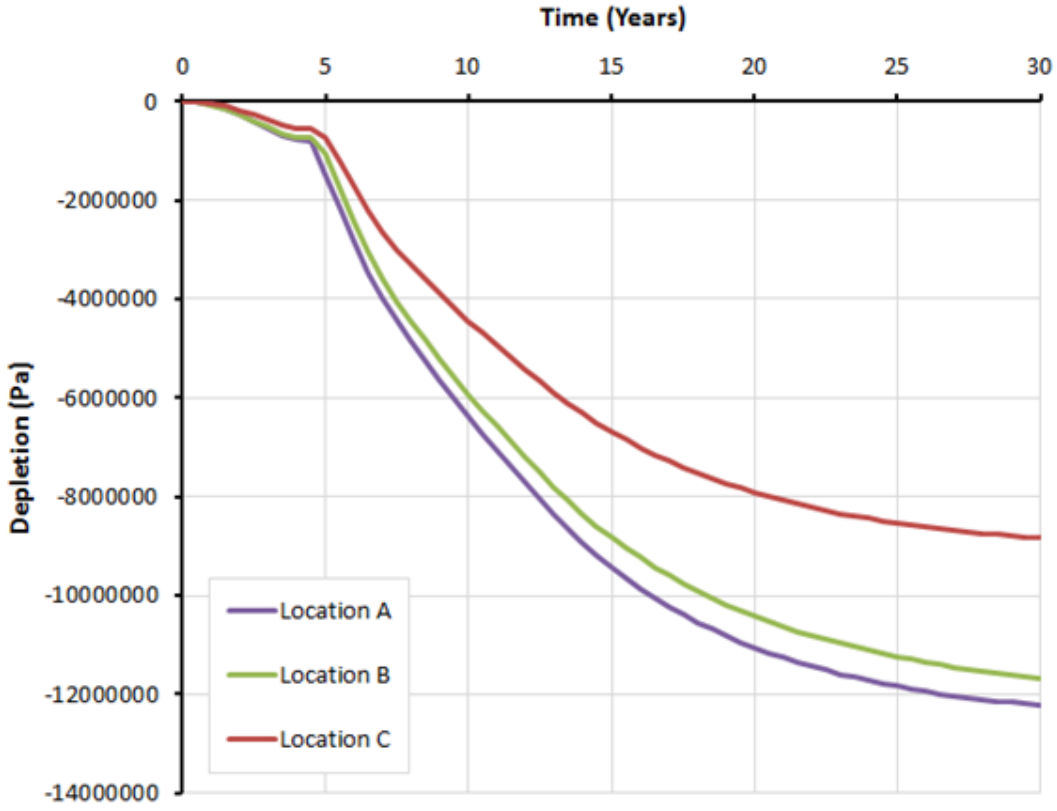
Time (Years)
0
5
10
15
20
25
30
0
-2000000
-4000000
-6000000
-8000000
-10000000
-12000000
-14000000
Depletion (Pa)
Location A
Location B
Location C

Figure 11

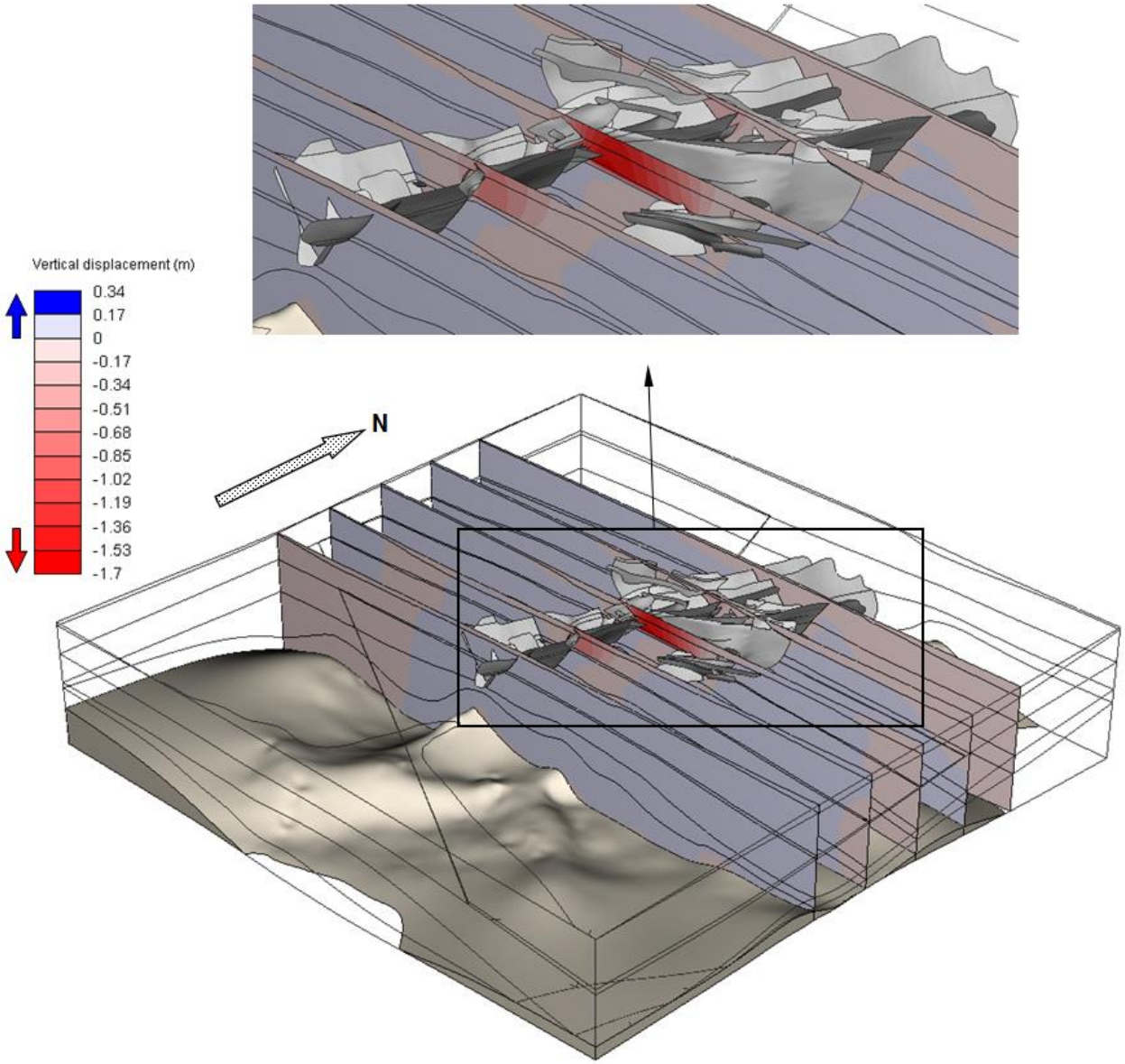
Vertical displacement (m)
0.34
0.17
0
-0.17
-0.34
-0.51
-0.68
-0.85
-1.02
-1.19
-1.36
-1.53
-1.7
N

Figure 12

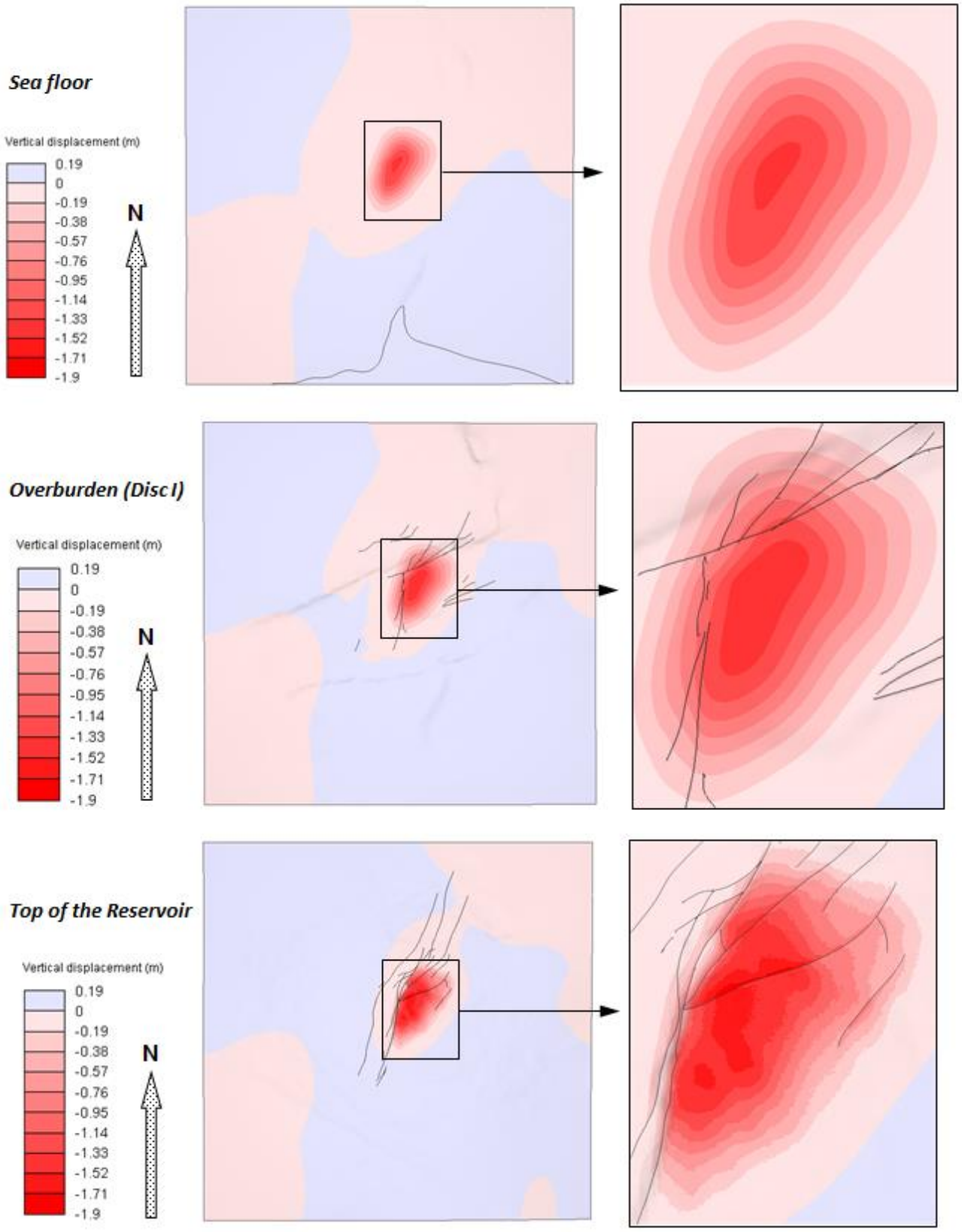
Sea floor
Vertical displacement (m)
0.19
0
-0.19
-0.38
-0.57
-0.76
-0.95
-1.14
-1.33
-1.52
-1.71
-1.9
N
Overburden (Disc I)
Vertical displacement (m)
0.19
0
-0.19
-0.38
-0.57
-0.76
-0.95
-1.14
-1.33
-1.52
-1.71
-1.9
N
Top of the Reservoir
Vertical displacement (m)
0.19
0
-0.19
-0.38
-0.57
-0.76
-0.95
-1.14
-1.33
-1.52
-1.71
-1.9
N

Figure 13

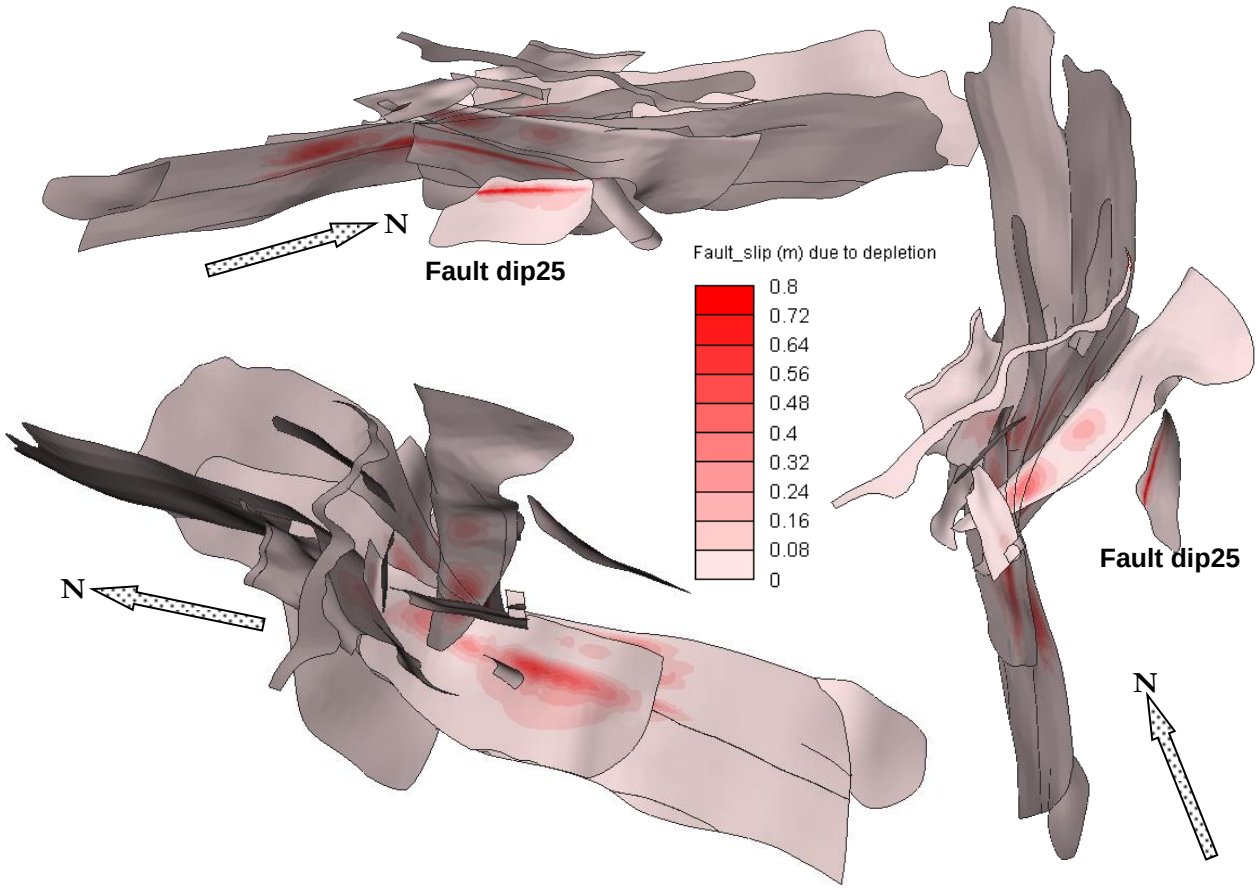
N
Fault dip25
Fault_slip (m) due to depletion
0.8
0.72
0.64
0.56
0.48
0.4
0.32
0.24
0.16
0.08
0
N
Fault dip25
N

Figure 14

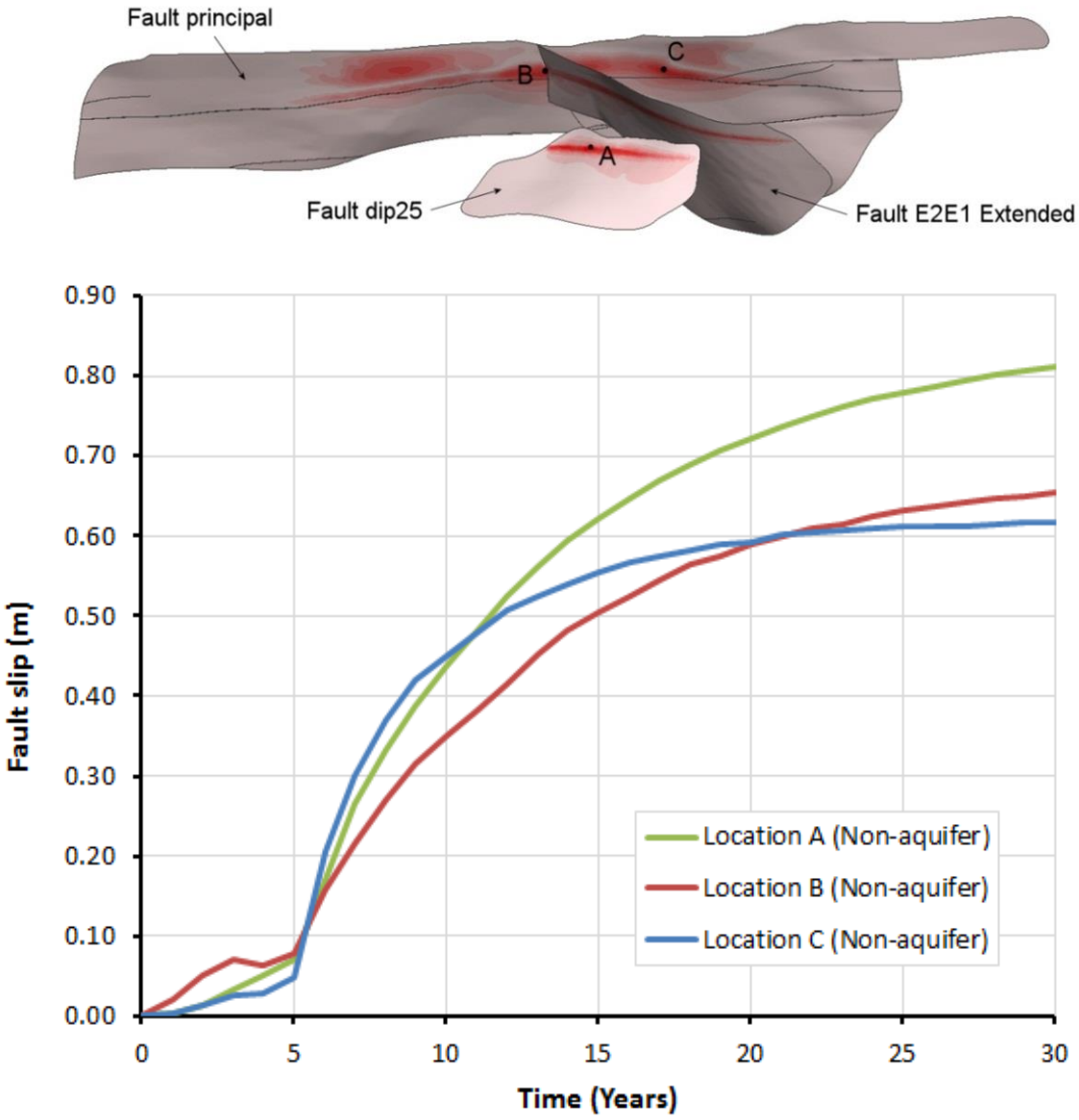
Fault principal
C
B
A
Fault dip25
Fault E2E1 Extended
0.90
0.80
0.70
0.60
0.50
0.40
0.30
0.20
0.10
0.00
Fault slip (m)
0
5
10
15
20
25
30
Time (Years)
Location A (Non-aquifer)
Location B (Non-aquifer)
Location C (Non-aquifer)

Figure 15

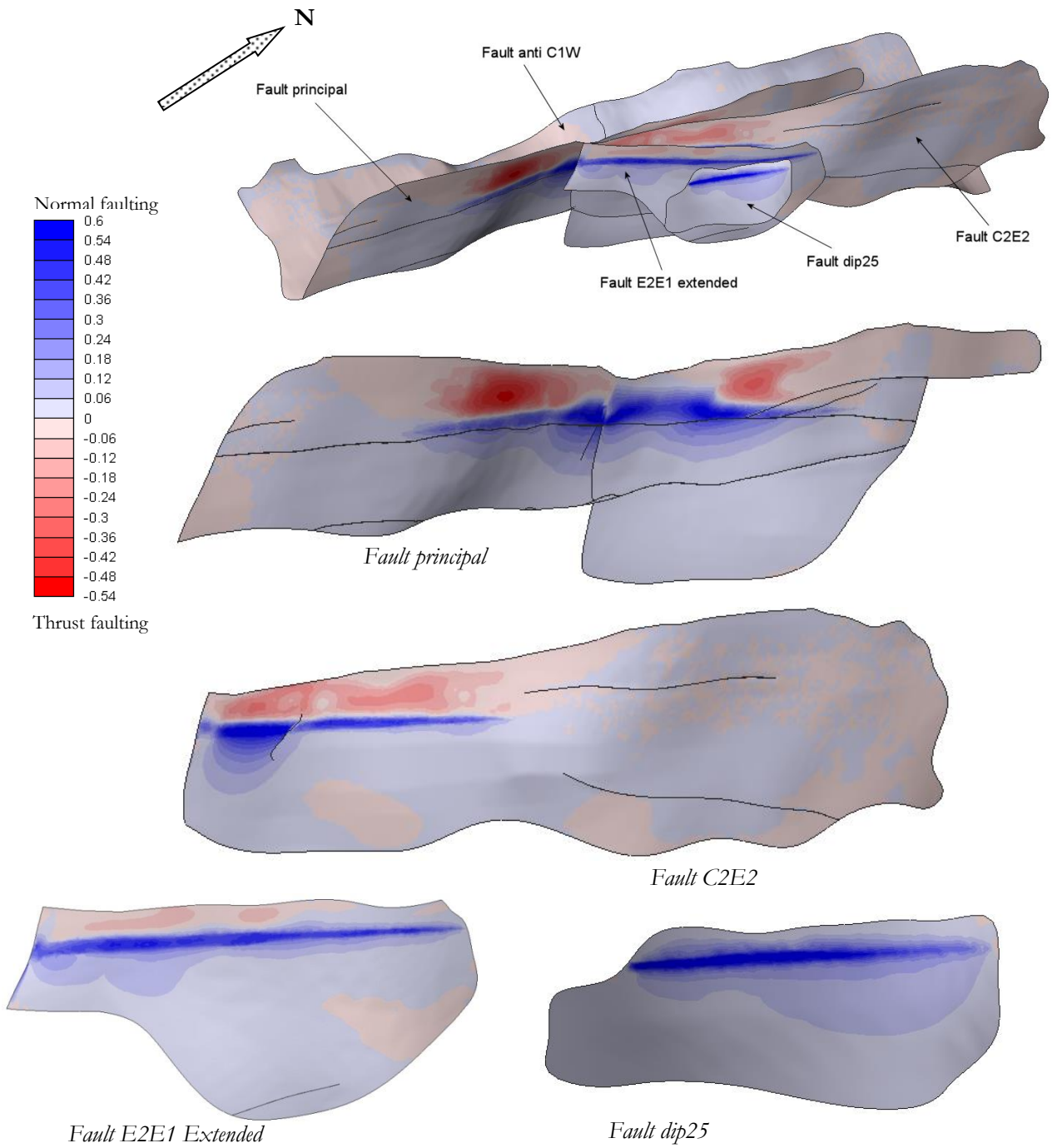
N
Fault anti C1W
Fault principal
Fault C2E2
Fault dip25
Fault E2E1 extended
Normal faulting
0.6
0.54
0.48
0.42
0.36
0.3
0.24
0.18
0.12
0.06
0
-0.06
-0.12
-0.18
-0.24
-0.3
-0.36
-0.42
-0.48
-0.54
Thrust faulting
Fault principal
Fault C2E2
Fault E2E1 Extended
Fault dip25

Figure 16

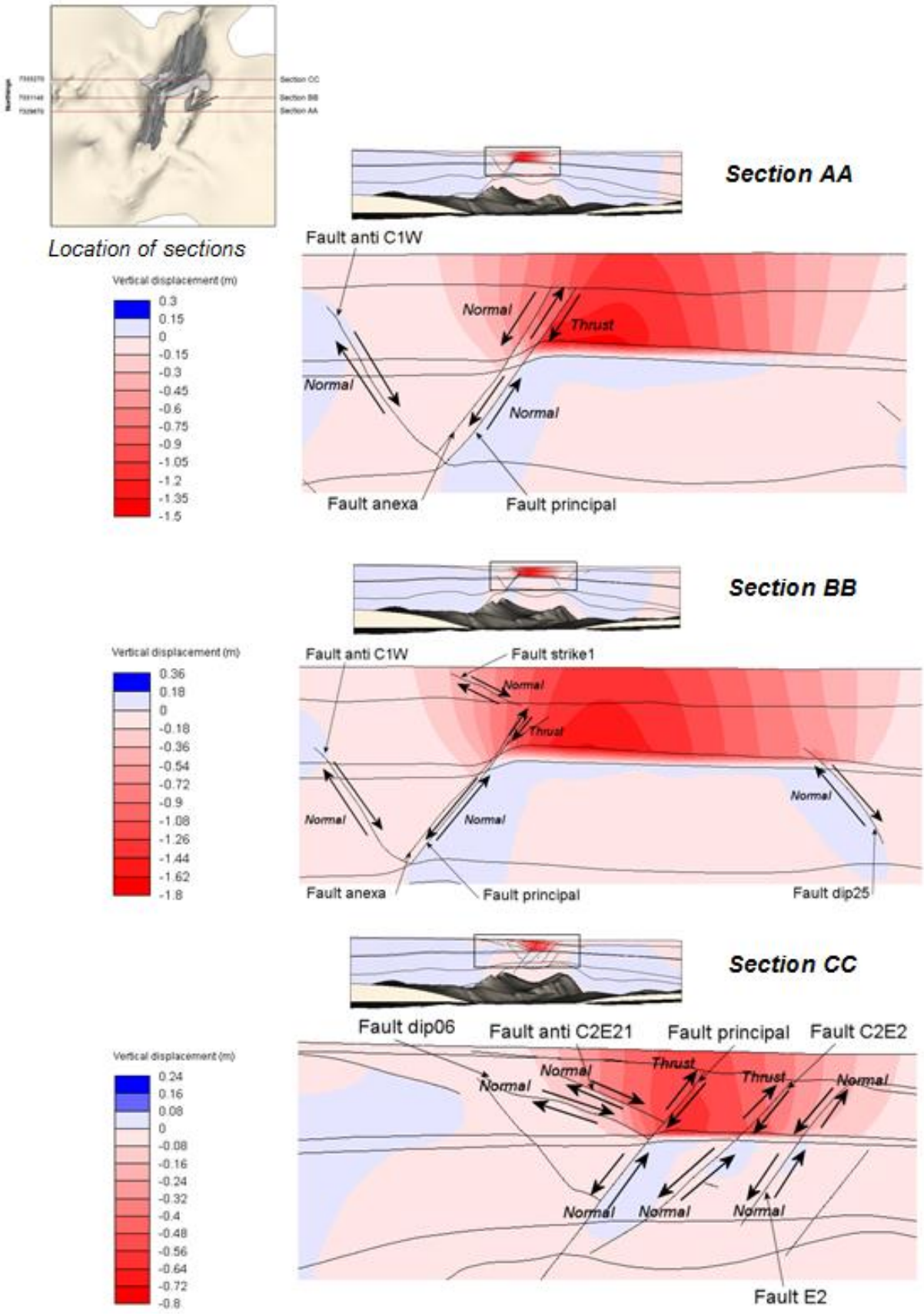
Section CC
Section BB
Section AA
Location of sections
Section AA
Vertical displacement (m)
0.3
0.15
0
-0.15
-0.3
-0.45
-0.6
-0.75
-0.9
-1.05
-1.2
-1.35
-1.5
Fault anti C1W
Normal
Thrust
Normal
Normal
Fault anexa
Fault principal
Section BB
Vertical displacement (m)
0.36
0.18
0
-0.18
-0.36
-0.54
-0.72
-0.9
-1.08
-1.26
-1.44
-1.62
-1.8
Fault anti C1W
Fault strike1
Normal
Thrust
Normal
Normal
Normal
Fault anexa
Fault principal
Fault dip25
Section CC
Vertical displacement (m)
0.24
0.16
0.08
0
-0.08
-0.16
-0.24
-0.32
-0.4
-0.48
-0.56
-0.64
-0.72
-0.8
Fault dip06
Fault anti C2E21
Fault principal
Fault C2E2
Normal
Normal
Thrust
Thrust
Normal
Normal
Normal
Normal
Fault E2

Figure 17

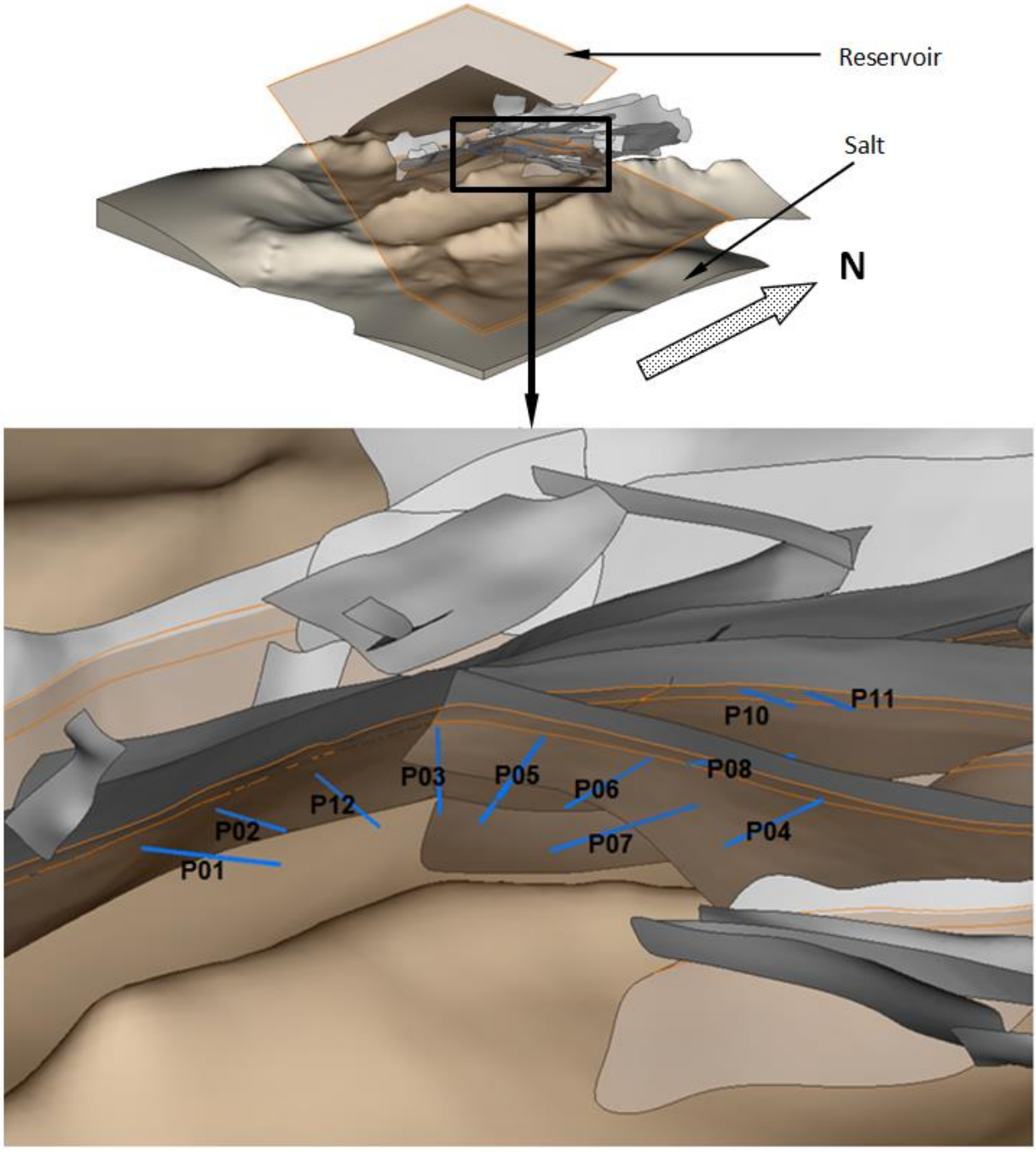

Figure 18

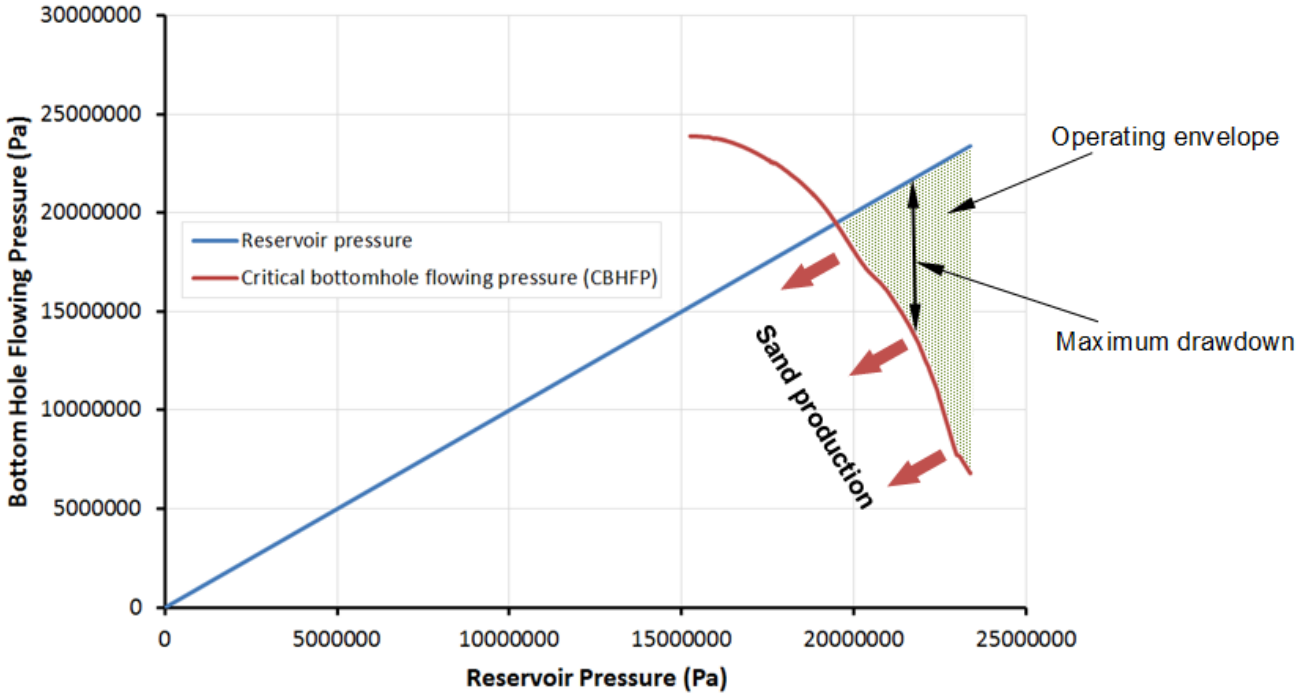
30000000
25000000
20000000
15000000
10000000
5000000
0
Bottom Hole Flowing Pressure (Pa)
0
5000000
10000000
15000000
20000000
25000000
Reservoir Pressure (Pa)
Reservoir pressure
Critical bottomhole flowing pressure (CBHFP)
Operating envelope
Maximum drawdown
Sand production

Figure 19

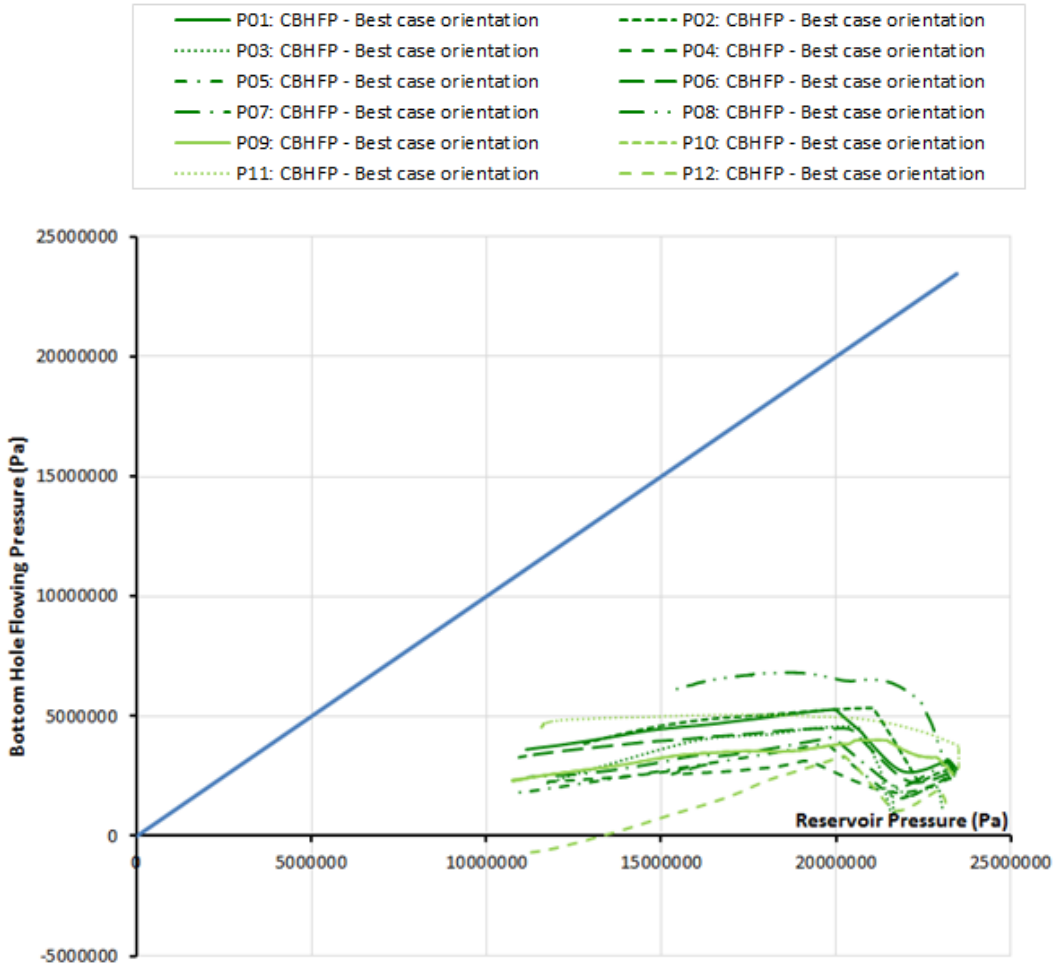
P01: CBHFP - Best case orientation
P02: CBHFP - Best case orientation
P03: CBHFP - Best case orientation
P04: CBHFP - Best case orientation
P05: CBHFP - Best case orientation
P06: CBHFP - Best case orientation
P07: CBHFP - Best case orientation
P08: CBHFP - Best case orientation
P09: CBHFP - Best case orientation
P10: CBHFP - Best case orientation
P11: CBHFP - Best case orientation
P12: CBHFP - Best case orientation
Bottom Hole Flowing Pressure (Pa)
Reservoir Pressure (Pa)
25000000
20000000
15000000
10000000
5000000
0
-5000000
0
5000000
10000000
15000000
20000000
25000000

Figure 20

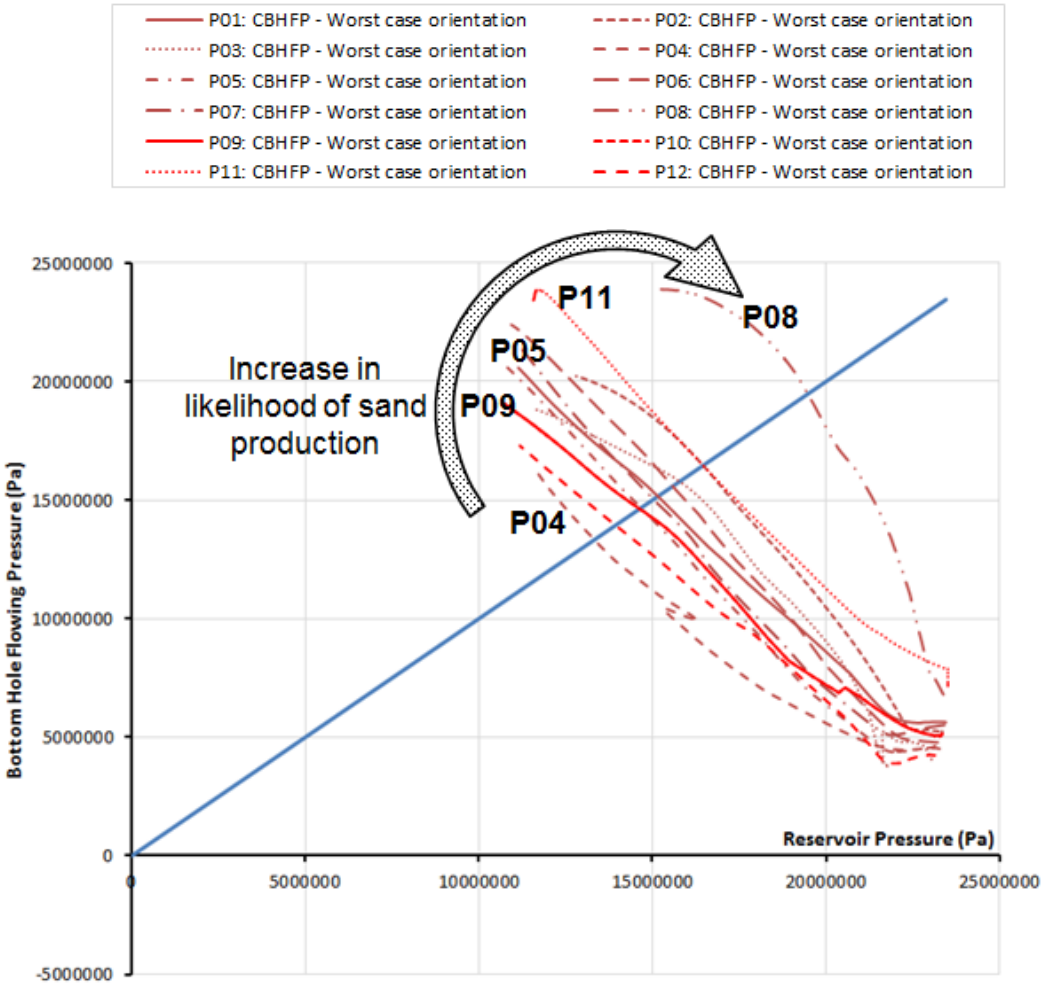
P01: CBHFP - Worst case orientation
P02: CBHFP - Worst case orientation
P03: CBHFP - Worst case orientation
P04: CBHFP - Worst case orientation
P05: CBHFP - Worst case orientation
P06: CBHFP - Worst case orientation
P07: CBHFP - Worst case orientation
P08: CBHFP - Worst case orientation
P09: CBHFP - Worst case orientation
P10: CBHFP - Worst case orientation
P11: CBHFP - Worst case orientation
P12: CBHFP - Worst case orientation
Increase in likelihood of sand production
P11
P08
P05
P09
P04
Bottom Hole Flowing Pressure (Pa)
Reservoir Pressure (Pa)
25000000
20000000
15000000
10000000
5000000
0
-5000000
0
5000000
10000000
15000000
20000000
25000000

Figure 21

List of Table Captions

Tables

Stratigraphy	TVDMSL (m) *1–SHEL–4/4A*	Upper and Lower Bounding Horizons
Unconsolidated mud	1550 – 1600	Sea Floor
		Unconsolidated Mud
Overburden	1600 – 2328.8	Unconsolidated Mud
		Disc I
		Disc II
		Eocene Top
Reservoir	2328.8 – 2442.5	Reservoir Top
		Reservoir Top
		Reservoir Base
Underburden (Upper)	2442.5 – 3368.0	Reservoir Base
		Cretaceous Top
		Disc III
		Disc IV
Underburden (Lower)	3368.0 –3970.9	Disc IV
		Albian Top
Albian	3970.9 –5214.5	Albian Top
		Salt Top
Salt	5214.5 – 6231.3	Salt Top
		Salt Base

Table 1

Material Name	Description (Griffiths, 2001)	Max/Min TVDMSL; Range (m) [Seabed 1070-1827]	Densities (kg/m^3)		Porosity		Elastic Properties			
							Young's Modulus (MPa)		Poisson's Ratio	
			Grain	Fluid	Lower Bound	Upper Bound	Lower Bound	Upper Bound	Lower Bound	Upper Bound
Unconsolidated mud	Top 50m	1070-1840; 770	2790	1025	0.64	0.58	3.0	5.25	0.15 (Assumed)	
Overburden	Fairly monotinous claystones, homogeneous and silty in places	1136-3678; 2542	2651	1071	0.42	0.38	200	500	0.38	0.30
Reservoir	Highly poroous unconsolidated sands; interbeds of claystones	2251-3846; 1595	2650	1071	0.37	0.30	600 (Assumed)	2000 (Assumed)	0.39 (Assumed)	0.29 (Assumed)
Underburden (Upper)	Graduation between Eocene sands above and claystones of underlying Maastrichtian	2365-5703; 3338	2651	1071	0.41-0.30	0.36-0.15	600 - 5000 [8]	2000-7000 [8]	0.39 [8]	0.29 [8]
Underburden (Lower)	Sand, silt, claystone and limestone interbedded sequence. Sands dominate upper section; claystones dominate lower section	3175-6685; 3510	2651	1071	0.30	0.10	5000	10000	0.33	0.27
Albian	Sand dominated formation with silty claystones as interbeds; towards the base limestones start to appear and dominate at times	3320-6780; 3460	2651 (Assumed)	1071 (Assumed)	0.30 (Assumed)	0.10 (Assumed)	7000 (Assumed)	12000 (Assumed)	0.30 (Assumed)	0.25 (Assumed)

Table 2

Material	Angles +ve anti-clockwise from EW axis and given in ()	
	K_H	K_h
Overburden	0.7 (60°)	0.53 (-30°)
Reservoir	0.7 (60°)	0.53 (-30°)
Underburden (Upper)	0.7 (–)	0.7 (–)
Underburden (Lower)	0.9 (-30°)	0.8 (60°)
Albian	0.9 (-30°)	0.8 (60°)
Salt	1.0 (–)	1.0 (–)

Table 3

		Minimum compressive total principal stress		Fracture gradient	
		(MPa)	(psi)	(psi/ft)	Error (%)
Minifrac test result		26.786	3885	0.5097 0.5090 0.5088	–
3D Model	2317m TVD	27.23	3949	0.5196	1.7
	2327m TVD	27.75	4025	0.5272	3.6
	2332m TVD	27.77	4028	0.5264	3.7

Table 4